tvst

Retina

Fluorescence Lifetime Imaging Ophthalmoscopy of Mouse Models of Age-related Macular Degeneration

Svenja Rebecca Sonntag[1], Britta Klein[2,3], Ralf Brinkmann[2,3], Salvatore Grisanti[1], and Yoko Miura[1–3]

[1] Department of Ophthalmology, University Hospital Schleswig-Holstein, Campus Lübeck, Lübeck, Germany
[2] Institute of Biomedical Optics, University of Lübeck, Lübeck, Germany
[3] Medical Laser Center Lübeck, Lübeck, Germany

Correspondence: Yoko Miura, Institute of Biomedical Optics, University of Lübeck, Peter-Monnik-Weg 4, Lübeck 23562, Germany. e-mail: yoko.miura@uni-luebeck.de

Received: July 23, 2023
Accepted: December 21, 2023
Published: January 29, 2024

Keywords: age-related macular degeneration; fluorescence lifetime imaging; mouse models; metabolic change; oxidative stress

Citation: Sonntag SR, Klein B, Brinkmann R, Grisanti S, Miura Y. Fluorescence lifetime imaging ophthalmoscopy of mouse models of age-related macular degeneration. Transl Vis Sci Technol. 2024;13(1):24, https://doi.org/10.1167/tvst.13.1.24

Purpose: To investigate fluorescence lifetime of mouse models of age-related macular degeneration (AMD) by fluorescence lifetime imaging ophthalmoscopy (FLIO).

Methods: Two AMD mouse models, apolipoprotein E knockout ($ApoE^{-/-}$) mice and NF-E2-related factor-2 knockout ($Nrf2^{-/-}$) mice, and their wild-type mice underwent monthly ophthalmic examinations including FLIO from 3 months of age. After euthanasia at the age of 6 or 11 months, blood plasma was collected to determine total antioxidant capacity and eyes were enucleated for Oil red O (ORO) lipid staining of chorioretinal tissue.

Results: In FLIO, the mean fluorescence lifetime (τ_m) of wild type shortened with age in both spectral channels. In short spectral channel, τ_m shortening was observed in both AMD models as well, but its rate was more pronounced in $ApoE^{-/-}$ mice and significantly different from the other strains as months of age progressed. In contrast, in long spectral channel, both model strains showed completely opposite trends, with τ_m becoming shorter in $ApoE^{-/-}$ and longer in $Nrf2^{-/-}$ mice than the others. Oil red O staining at Bruch's membrane was significantly stronger in $ApoE^{-/-}$ mice at 11 months than the other strains. Plasma total antioxidant capacity was highest in $ApoE^{-/-}$ mice at both 6 and 11 months.

Conclusions: The two AMD mouse models exhibited largely different fundus fluorescence lifetime, which might be related to the different systemic metabolic state. FLIO might be able to indicate different metabolic states of eyes at risk for AMD.

Translational Relevance: This animal study may provide new insights into the relationship between early AMD-associated metabolic changes and FLIO findings.

Introduction

Age-related macular degeneration (AMD) is one of the most common causes of visual impairment in industrialized countries.[1] Clinical indicators of AMD include lipid deposits such as drusen, choroidal neovascularization, and atrophic alterations. Pathogenesis of AMD is promoted by systemic and functional disorders, such as defective regulation of the immune system, disorders of lipid transports or oxidative stress.[2–5] The decrease in metabolism and function of retinal pigment epithelial (RPE) cells and photoreceptor cells caused by these factors is thought to precede structural changes as early changes toward AMD.[3,6,7] However, these abnormalities cannot be clinically confirmed to date. Early detection may increase the possibility of establishing prevention methods, and thus there is a strong need for methods to detect these early alterations.

Fluorescence lifetime imaging ophthalmoscopy (FLIO) is a new diagnostic tool that noninvasively measures the fluorescence lifetime (FLT) of retinal intrinsic fluorophores.[8–10] FLT, usually in the range of picoseconds to nanoseconds, can be altered not only by changes in the composition of fluorophores owing to structural changes in fundus tissue, but also by metabolic changes.[11] Therefore, it is expected to

detect early metabolic changes in degenerative retinal disorders, such as diabetic retinopathy and AMD. In fact, Schweitzer et al.[12] presented the changed FLT in diabetic patients who do not exhibit any apparent diabetic retinopathy, and Sauer et al.[13] discovered the specific FLT changes in patients with early AMD. Recently, we have reported differences in FLT between young adult smokers and nonsmokers.[14] Because smoking is known to impair mitochondria function and to be one of the risk factors of ocular diseases, including AMD, this result strongly indicates that FLIO might be able to capture early indicators of certain diseases.

However, the correlation between early pathologies of AMD and the alterations in FLT is not yet understood fully. Therefore, in this study, we investigated the fundus FLT of two mouse models that have long been used as models in AMD research over time: apolipoprotein E knockout ($ApoE^{-/-}$) mice with genetic mutations, which cause impaired systemic lipid transport and elevated serum triglycerides und cholesterol,[15] and nuclear factor erythroid 2-related factor 2 (NRF2) knockout ($Nrf2^{-/-}$) mice lacking a transcription factor for antioxidant and detoxification responses by NRF2,[16] beginning in the early period after birth.

Methods

Animals

The inbred strain C57BL/6J mice (B6; wild type [WT]) was investigated as control and two different transgenic mice, apolipoprotein E knockout ($ApoE^{-/-}$) mice (B6.129P2-$Apoe^{tm1Unc}$/J, JAX stock #002052)[17] and Nrf2 knockout ($Nrf2^{-/-}$) mice (B6.129X1-$Nfe2l2^{tm1Ywk}$/J, JAX stock #017009)[18] were investigated as the mouse models of AMD. All mice were purchased from The Jackson Laboratory (Bar Harbor, ME) via the provider Charles River Laboratory ('s-Hertogenbosch, the Netherlands). The animal study was approved by the Ethics Committee of the Ministry of Energy, Agriculture, Environment, Nature and Digitalization and followed the guidelines for the Use of Animals in Ophthalmic and Vision Research promulgated by the Association for Research in Vision and Ophthalmology.

A total of 72 female mice (24 WT, 24 $ApoE^{-/-}$, and 24 $Nrf2^{-/-}$) at the age of 6 to 8 weeks were shipped. During the study period, animals were kept at a regular circadian cycle and constant room temperature with free access to drinking water and food (ad libitum). Four mice were kept in each cage.

Experimental Design

Ocular examinations, including slit lamp examination, fundoscopy, optical coherence tomography (OCT), and FLIO, were performed on a monthly basis during the examination period. As described in Figure 1, one-third of each strain (8 mice) were investigated from the 3rd to the 6th months of life, another one-third (8 mice of each strain) were investigated from the 3rd to the 11th months of life, the remaining one-third (8 mice of each strain) were investigated from the 7th to the 11th months of life. The mice in the first group were euthanized after the measurements in the 6th month, whereas the mice in the second and the third groups were euthanized after the investigations in the 11th month. The mice of the third group were kept in the cage without being investigated until their examination period began in the 7th month. At the time of euthanasia, the eyes were enucleated and blood was collected from all mice.

Anesthesia and Preparations for Measurement

All measurements were undertaken under general anesthesia with an intraperitoneal injection of 65 mg/kg ketamine (50 mg/mL ketamine, belapharm GmbH & Co. KG, Vechta, Germany) and 0.75 mg/kg medetomidine (Dorbene vet: 1 mg/mL, Laboratories SYVA, S.A.U., León, Spain). Pupils were dilated using eye drops containing methyl cellulose (Methocel 2%; OmniVision, Neuhausen am Rheinfall, Germany), isotonic saline solution (Fresenius Saline Solution 0.9% Pl. Fresenius Amp.; Fresenius Kabi, Bad Homburg vor der Höhe; Germany), and a suspension of tropicamide 0.5% and phenylephrine HCl 2.5% (Mydriasis Sine AD, UKSH Pharmacy, Lübeck, Germany) in a 10:10:1 proportion. Before measurement, the cornea was constantly moistened with a 1:1 mixture of isotonic saline solution and methyl cellulose to prevent corneal drying. During measurements the solution was replaced by isotonic salt solution without methyl cellulose. After completion of the measurements but at least half an hour after the injection of the anesthetics, the effect of medetomidine was reversed with the intraperitoneal injection of 2.5 mg/kg Atipamezol (Alzane: 5 mg/mL, Laboratories SYVA, S.A.U.). To avoid injuries from cage mates, the animals were kept in isolation until their complete recovery. During anesthesia heating pads with a temperature of 37°C were used to prevent a decline in body temperature.

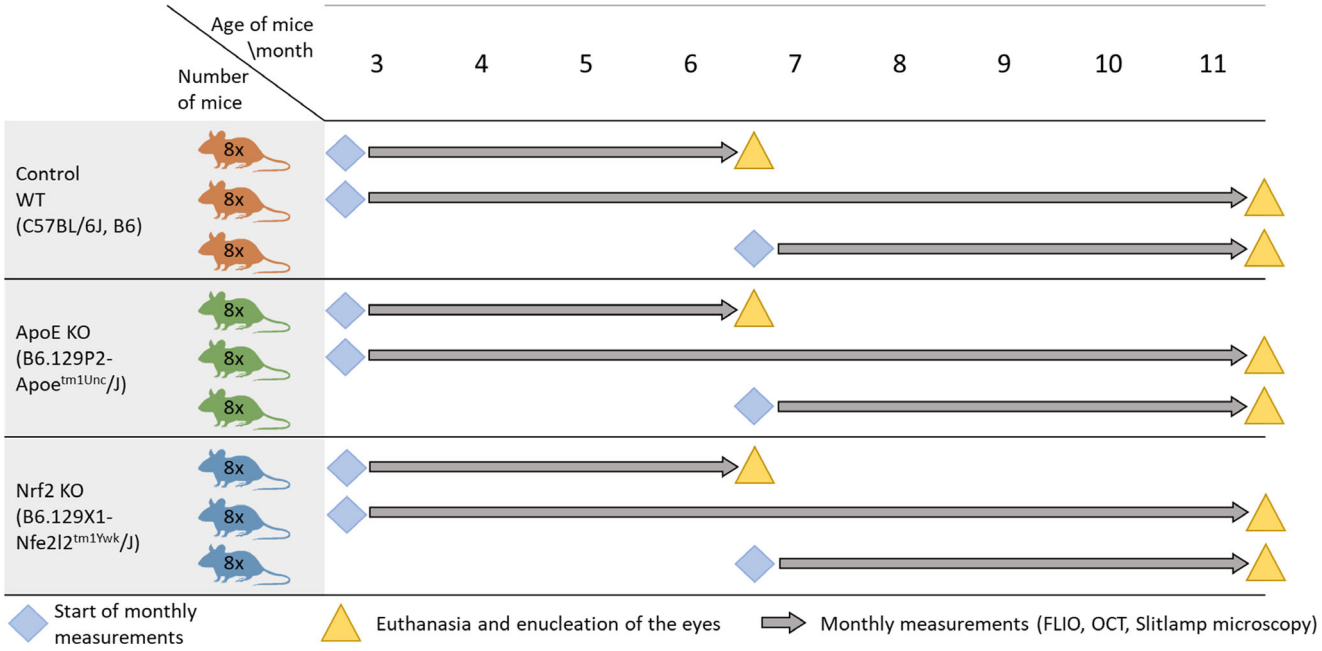

Figure 1. Schematic description of the animal experiment. Eight of the 24 animals of each group underwent FLIO, OCT, and slit lamp examination from month 3 to month 6, 8 animals were examined from month 7 to month 11, and the rest of the animals were examined over the whole time period. After the last examination at the different time points each animal was euthanatized and enucleated. Furthermore, blood samples were collected.

Slit Lamp Microscopy

A slit lamp examination was performed using a portable slit lamp (LS-1, SunKingdom Medical, Chongqing, China) at the beginning and end of each measurement to detect possible changes in the anterior segment of the eye like cataract formation or corneal injuries. Any damage to the anterior segment of the eye or the lens was noted and in severe cases the images were excluded from evaluation.

FLIO

The FLT of the fundus autofluorescence was measured with FLIO (Heidelberg Engineering GmbH, Heidelberg, Germany). FLIO uses a picosecond (70 ps)-pulsed excitation laser (λ_{ex} = 473 nm) with a repetition rate of 80 MHz. Two highly sensitive hybrid detectors (HPM-100-40; Becker & Hickl GmbH, Berlin, Germany) register the detected emission light in a short spectral channel (SSC) (498–560 nm) and a long spectral channel (LSC) (560–720 nm). These spectral detectors are connected to time-correlated single photon counting module (SPC-150, Becker & Hickl). An infrared laser (λ_{ex} = 815 nm) eye tracking system is equipped to compensate for eye movements during measurement.

After slit lamp examination, FLIO was conducted. To compensate for the different axial length of the mouse eye a 25 diopter (D) lens (f = 40/+25 D, Heidelberg Engineering GmbH) was adjusted in front of the camera of the FLIO system. The mice were placed on a table mounted horizontally in front of the camera lens (Fig. 2A). All mice were positioned so that the optic nerve was visible in the center of the image. To avoid drying of the cornea, the eye was treated with isotonic salt solution before measurement. Image acquisition took place in a darkened room until on average 1000 photons per pixel were detected, with acquisition time ranging from 1.5 to 3.0 minutes.

For analysis of the detected photon counts the data was processed with the software SPCImage (version 4.4.2, Becker & Hickl).[19] Using this software, the fluorescence decay was fitted to a biexponential curve with pixel binning 1 (3 × 3). This curve can be described by the sum of its exponential components:

$$f(t) = \sum_{n=1}^{2} \alpha_i \cdot e^{-t/\tau_i},$$

where τ_1 and τ_2 describe the FLTs of short and long exponential components, respectively, and α_1 and α_2 describe the corresponding amplitudes. Furthermore, the software SPCImage calculates the mean FLT τ_m of

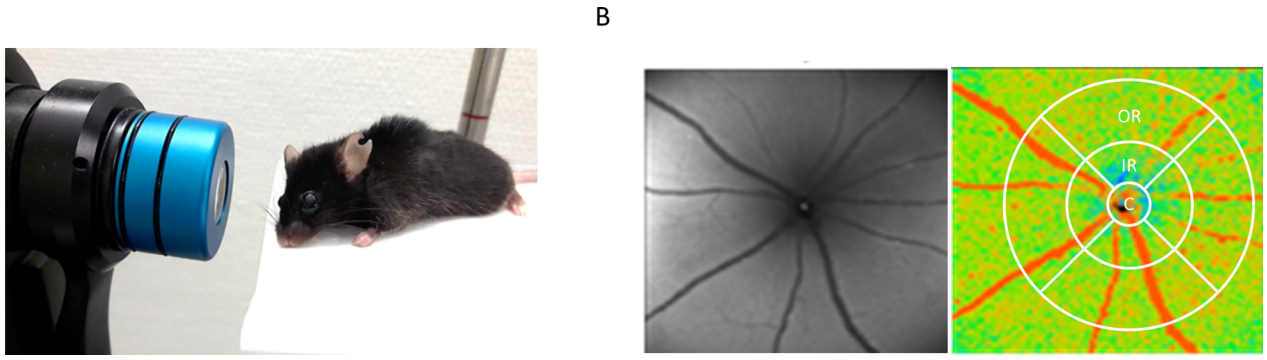

Figure 2. FLIO with mice. (**A**) Mouse in front of the FLIO device. Because of the short eye of the mouse a 25 D lens (blue) was positioned in front of the FLIO camera. (**B**) FLIO image and the grid for analysis. In FLIO, infrared reflection image (*left*) and the pseudo-colored FLT images (*right*) are provided. The FLIO data was analyzed by the FLIO Reader software, which uses an Early Treatment Diabetic Retinopathy Study grid consisting of a central region (**C**), inner ring (IR) and outer ring (OR). In this study, the optic nerve head was placed in (**C**).

a biexponential fitting model as follows:

$$\tau_m = \frac{\alpha_1 \cdot \tau_1 + \alpha_2 \cdot \tau_2}{\alpha_1 + \alpha_2}.$$

The goodness of fit was assessed with reduced chi-squared (χ^2). To calculate an average value of τ_m for a circular area around the optic nerve disc the processed data was then transferred to the software FLIO reader (ARTORG Center for Biomedical Engineering Research, University of Bern, Switzerland). FLIO reader uses an Early Treatment Diabetic Retinopathy Study grid, which is divided into a central area, outer ring, and inner ring (Fig. 2B). The circular diameter of outer ring and inner ring was set approximately to 3600 µm and 1800 µm, respectively, and 600 µm for the central area.[20] For this study, the Early Treatment Diabetic Retinopathy Study grid was centered over the head of the optic nerve. For data analysis, only data from the inner ring were included. The usability of this ring area around the optic nerve disc has been already proven in previous studies.[20,21]

OCT

Directly after FLIO, OCT was conducted using an OCT system (Spectralis, Heidelberg Engineering GmbH). The mouse was placed on a stage set in front of the OCT device. The additional 25 D lens was used to focus on the mice retina as done in FLIO. OCT was performed using a scan pattern with a size of 20° × 20° centered around the optic disc, which records 49 B-scans per eye.

Blood Analysis

The mice were euthanized by a final blood sampling from the right ventricle under deep terminal anesthesia. Blood of each mouse was collected in different microvettes with heparin (Microvette CB 300 µL, Lithium-Heparin, orange EU-Code, Sarstedt AG & Co. KG, Nümbrecht, Germany). To separate the blood plasma, the whole blood was placed at room temperature for 3 to 4 hours, followed by centrifugation at a speed of 2000×*g* for 5 minutes at 20°C. The supernatant plasma was collected and frozen at −80°C until use for the measurement of total antioxidant capacity (TAC) as described elsewhere in this article.

TAC

To assess the systemic antioxidant capacity, blood TAC was measured using a commercially available kit (Total Antioxidant Capacity Assay Kit, Abcam plc, Cambridge, UK). This colorimetric method is based on the reduction of Cu^{2+} to Cu^{+} by smaller oxidative molecules and proteins. Because the reduced Cu^{+} ion is chelated with a colorimetric probe with an absorbance peak around an optical density of 570 nm, an optical density at 570 nm is proportional to the TAC. All standards and samples were measured in duplicate. A reference curve was constructed using the antioxidant capacity of known concentrations of trolox (6-hydroxy-2,5,7,8-tetramethylchroman-2-carboxylic acid), and the antioxidant capacity of the examined sample was expressed in trolox equivalents antioxidant capacity (TEAC).

Oil Red O (ORO) Lipid Staining

Directly after euthanasia, the eyes of the mice were enucleated quickly and prepared for cryopreservation. Briefly, the eyes were washed in ice-cold phosphate-buffered saline (PBS) without calcium and magnesium and incubated in 4% phosphate-buffered formalde-

hyde solution (PFA, Carl Roth GmbH; Karlsruhe, Germany) for 30 minutes. The eyes were again washed with PBS and then transferred to a 5% sucrose–PBS solution and a 30% sucrose–PBS solution for 30 minutes and 1 hour, respectively, but at least until the eyes sank to the ground of the container. To avoid tissue irritation, the eyes were acclimatized to the preservative medium (Tissue-Tek O.C.T. Compound, Sakura Finetek, Alphen aan den Rijn, the Netherlands) in two steps (4:1 30% sucrose solution to O.C.T. Compound and 2:1 30% sucrose solution to O.C.T. Compound) for 30 minutes each. The eyes were then shock-frozen in individual cryomolds (Tissue Tek Cryomold Biopsy, Sakura Finetek) with O.C.T Compound using liquid nitrogen. They were stored at –80°C until examination.

To assess the lipid deposition, the cryopreserved eyes were cut by microtome in 10-µm slides and stained with ORO. The classical lysochromic liposoluble dye ORO binds to triglycerides, cholesteryl esters, free fatty acids and vitamin A esters.[22] The frozen–chorioretinal sections were treated with a 0.5% ORO (Merck KGaA, Darmstadt, Germany) solution (in 99% isopropanol) for 30 minutes at room temperature, followed by immersion in a 60% isopropanol solution for 12 minutes. Sections pretreated with Folch reagent (chloroform:methanol, 2:1) to extract lipids served as histochemical controls. The counterstain was performed with Mayer hematoxylin. After washing, slides were mounted with solution (Moviol, Sigma-Aldrich Chemie GmbH, Taufkirchen, Germany) and a glass coverslip and examined using a light microscope (Exlipse Ti, Nikon, Japan). Image analysis was performed by two raters masked to the mouse strain, who subjectively rated the intensity of ORO staining (red) of Bruch's membrane on a scale of 0 to 3. A score of 0 indicates no staining and a score of 3 indicates very strong staining.

Statistical Analysis

For all statistical work, the statistical software GraphPad Prism (version 9.3.1) was used. All FLIO data from all mice at every time point was analyzed by mixed model approach, which is comparable with a two-way analysis of variance. The mixed model approach allows for missing values in a dataset, such as images excluded from the analysis owing to bad corneal condition.

Furthermore, blood TAC values at 6 and 11 months of age for all groups were compared by Tukey's multiple comparison test after performing analysis of variance (normality was shown). To compare the scores for ORO staining among groups, Kruskal-Wallis test and Dunn's multiple comparison test (normality was not shown) were performed, between each point in time a Mann–Whitney test was used. Normality was tested by Shapiro–Wilk test. All results are provided as mean ± standard deviation.

Results

Number and Time of Animals' Drop Out

During the entire experimental period, a total number of 0 from WT, 0 from ApoE$^{-/-}$ mice, and two from Nrf2$^{-/-}$ mice (at months 5 and 9) were removed from the study and euthanized earlier than intended owing to health problems, including defective tooth growth and open wounds. Other animals lived through the entire experimental period without severe illness.

General Conditions

Body weight was measured monthly beginning in month 3. There was no significant difference in body weights from the initial month (3 months old) to the last month (11 months old) among the strains (Fig. 3). Furthermore, no differences were found between the groups measured from 3 months of age and from 7 months of age in all strains.

In detail, body weight at 3 months of age was 19.6 ± 1.3 g in WT mice, 19.5 ± 1.4 g in ApoE$^{-/-}$ mice, and 21.3 ± 1.4 g in Nrf2$^{-/-}$ mice, and at 11 months of age 27.8 ± 2.0 g in WT mice, 26.9 ± 1.3 g in ApoE$^{-/-}$ mice, and 26.8 ± 2.4 g in Nrf2$^{-/-}$ mice.

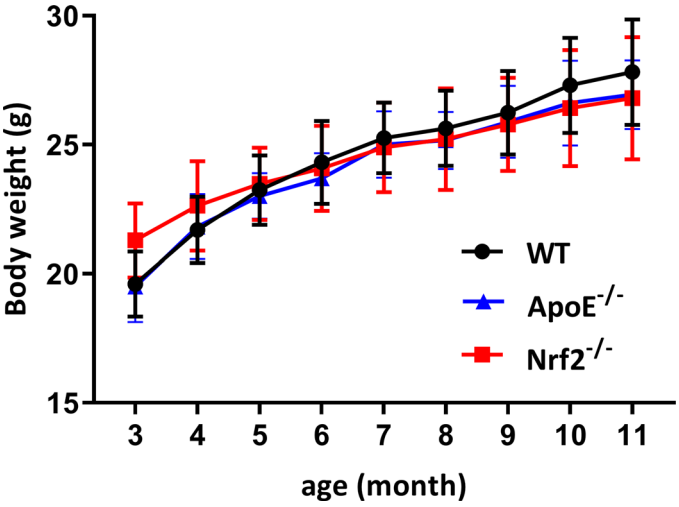

Figure 3. Change in body weight during the study period. Body weight was measured monthly with the beginning at month 3. There were no significant differences between the three strains.

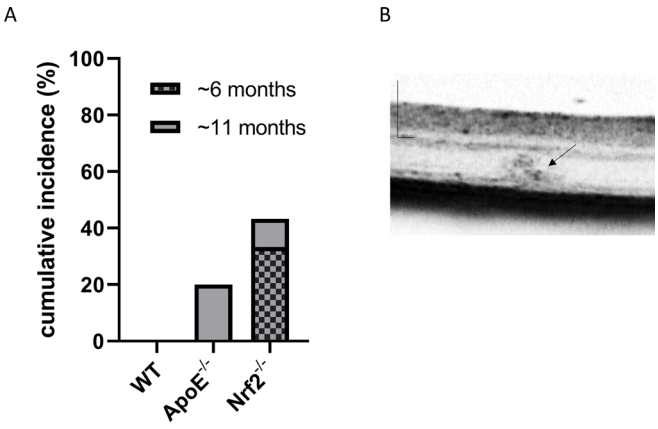

Figure 4. OCT findings over time. (**A**) Percentages of cumulative incidence of abnormality in OCT at 6 and 11 months. The graph shows the comparison of the cumulative incidence (%) of the mice showing abnormal changes in the outer retina in OCT. WT mice showed no changes during whole study period. Abnormality began to appear before month 6 in some Nrf2$^{-/-}$ mice and in the month 7 in some ApoE$^{-/-}$ mice, with 43% and 20% showing abnormal findings at 11 months of age, respectively. (**B**) An OCT image suggesting a proliferative change in the outer retina. Irregular and hyperreflective signal in the outer retina (*arrow*). Scale bar, 200 µm

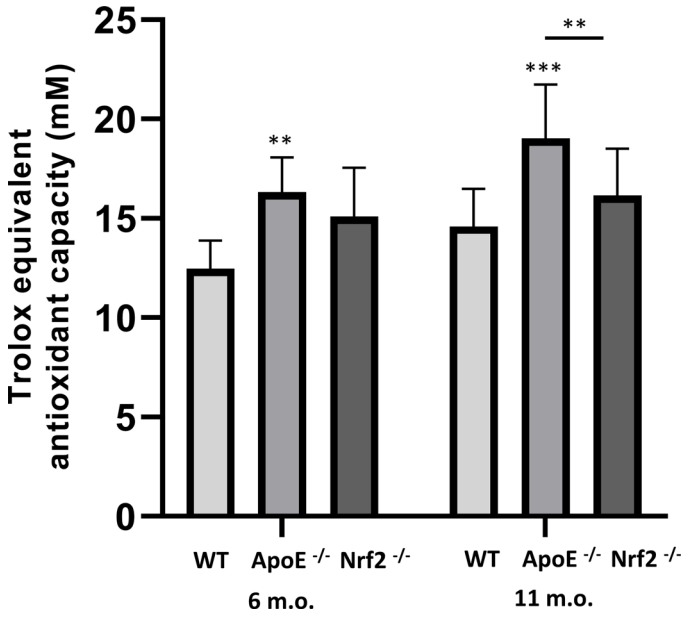

Figure 5. TEAC of blood plasma at months 6 and 11. Both at ages 6 and 11 months, ApoE$^{-/-}$ mice had significantly higher TAC than WT mice, and at 11 months, also significantly higher than Nrf2$^{-/-}$ mice. $^{**}P < 0.01$, $^{***}P < 0.001$, m.o.: month old.

Abnormality in OCT

Cumulatively, less than one-half of the AMD mouse models (43% in Nrf2$^{-/-}$ mice and 20% in ApoE$^{-/-}$ mice) showed structural abnormalities in the retina in OCT during the study period (Fig. 4A). The change was first detected at 4 months in Nrf2$^{-/-}$ mice and at 6 months in ApoE$^{-/-}$ mice. The main change was an abnormal, irregular, hyper-reflective signal in the outer retina, suggesting intraretinal proliferative changes (Fig. 4B). None of WT mice showed such apparent abnormalities in OCT at any point in time. Because fluorescein angiography was not conducted in this study, leakage without apparent morphological change could not be evaluated, but no signal indicating intraretinal or subretinal fluid accumulation was detected in any strain at any point in time.

TAC of Blood Plasma

Blood plasma from 6- and 11-month-old mice collected at the time of euthanasia was assessed for

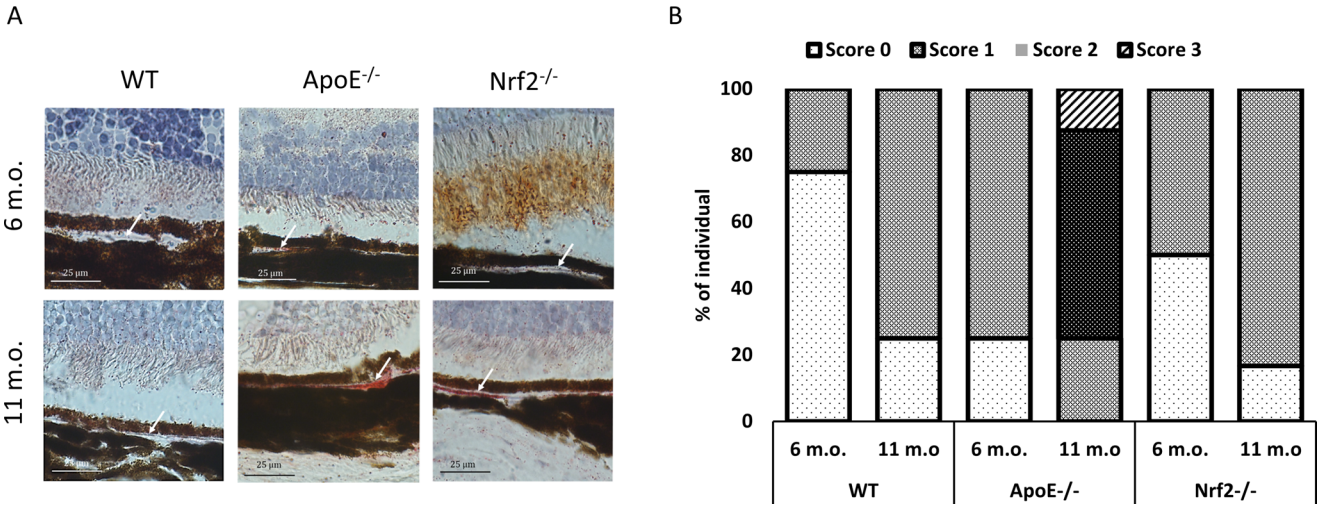

Figure 6. ORO staining of the Bruch's membrane. (**A**) Representative images of staining at months 6 and 11 for each strain. The red staining indicates the lipids stained with ORO at the Bruch's membrane (*arrows*). (**B**) ORO scores of each strain at months 6 and 11. Based on the staining results, the degree of staining was rated subjectively on a scale of 0 (no staining) to 3 (strong staining) (in 1-point increments).

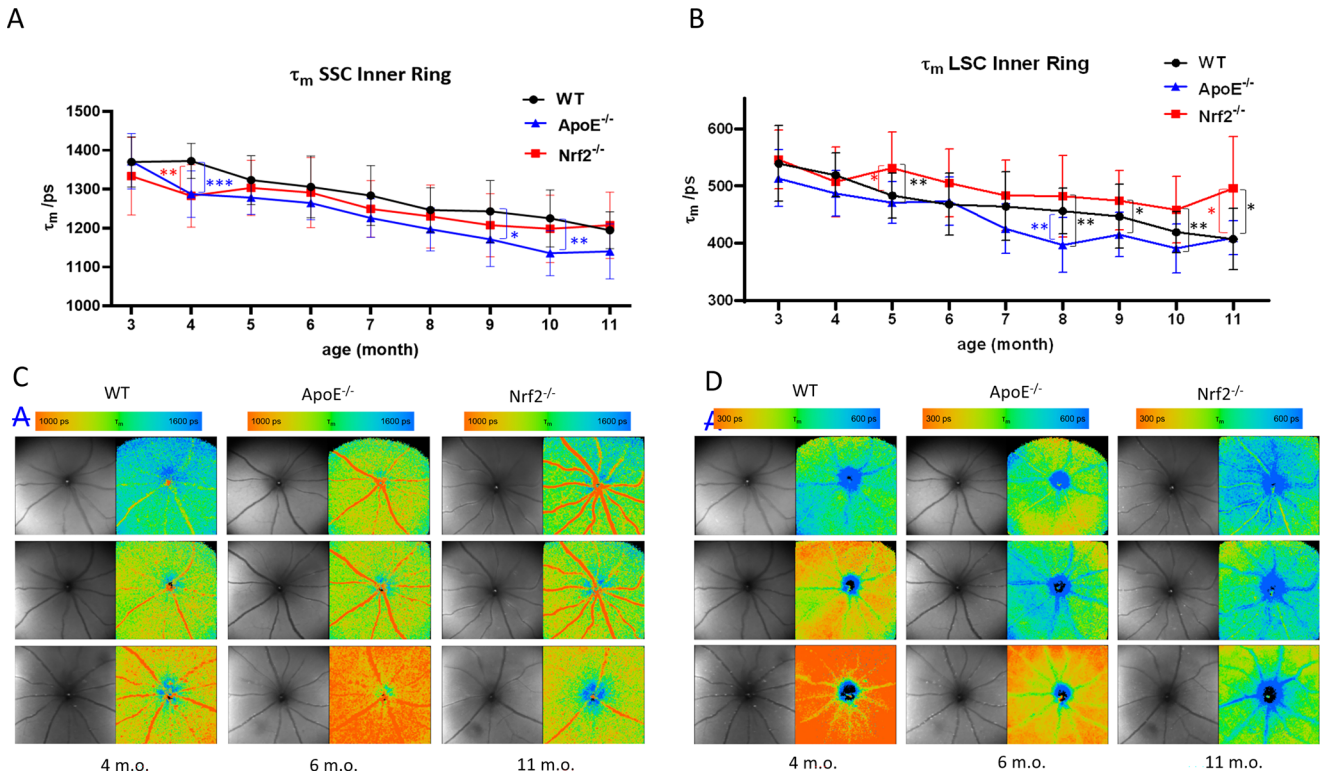

Figure 7. Comparison of τ_m changes over time in SSC and LSC from 3 to 11 months of age. (**A**) τ_m (mean ± standard deviation) in SSC. (**B**) τ_m (mean ± standard deviation) in LSC, $^*P < 0.05$, $^{**}P < 0.01$, $^{***}P < 0.001$ and representative FLIO images at months 4, 6, and 11 in SSC (**C**) and LSC (**D**). The concrete values for each time point and statistic results are shown in Tables 1–3.

TAC (Fig. 5). Generally, TEAC increased with age in all strains, where TEAC of ApoE$^{-/-}$ mice ($TEAC_{6m}$ = 16.33 ± 1.74 mM; $TEAC_{11m}$ = 19.03 ± 2.61 mM) was significantly higher than WT ($TEAC_{6m}$ = 12.47 ± 1.30 mM; $TEAC_{11m}$ = 14.59 ± 1.83 mM) at both times and also than the ones of Nrf2$^{-/-}$ mice ($TEAC_{6m}$ = 15.09 ± 2.46 mM; $TEAC_{11m}$ = 16.16 ± 2.36 mM) at 11 months.

Table 1. Monthly Measured τ_m Values (Mean, Standard Deviation) in SSC and LSC Over the Whole Study Period for all Three Strains

Age in Months	3 Months	4 Months	5 Months	6 Months	7 Months	8 Months	9 Months	10 Months	11 Months
τ_m SSC Mean (ps)									
WT (B6)	1370	1373	1324	1306	1284	1247	1243	1225	1195
ApoE$^{-/-}$	1372	1287	1278	1265	1226	1197	1171	1136	1140
Nrf2$^{-/-}$	1334	1283	1304	1291	1249	1230	1207	1198	1207
τ_m SSC SD (ps)									
WT (B6)	65	45	63	80	77	57	79	73	47
ApoE$^{-/-}$	71	60	43	43	50	55	69	58	71
Nrf2$^{-/-}$	100	80	71	90	72	81	81	86	85
τ_m LSC Mean (ps)									
WT (B6)	539	519	483	468	464	456	447	419	407
ApoE$^{-/-}$	513	487	471	473	425	397	415	391	409
Nrf2$^{-/-}$	546	507	532	505	483	482	475	459	496
τ_m LSC SD (ps)									
WT (B6)	66	38	40	54	60	40	56	36	54
ApoE$^{-/-}$	50	40	36	42	43	48	39	43	29
Nrf2$^{-/-}$	51	61	62	60	62	72	52	58	90

Table 2. Results of Statistical Analysis of τ_m Comparison Between Different Time Points in Each Strain

τ_m SSC

B6 (WT)	τ_m-SSC 3m	4m	5m	6m	7m	8m	9m	10m	11m
τ_m-SSC 3m		ns	ns	ns	ns	**	***	****	****
4m			ns	ns	*	****	****	****	****
5m				ns	ns	ns	*	**	****
6m					ns	ns	ns	*	***
7m						ns	ns	ns	*
8m							ns	ns	ns
9m								ns	ns
10m									ns
11m									

ApoE$^{-/-}$	τ_m-SSC 3m	4m	5m	6m	7m	8m	9m	10m	11m
τ_m-SSC 3m		ns	ns	*	***	****	****	****	****
4m			ns	ns	ns	*	***	****	****
5m				ns	ns	ns	**	****	****
6m					ns	ns	**	****	****
7m						ns	ns	*	*
8m							ns	ns	ns
9m								ns	ns
10m									ns
11m									

Nrf2$^{-/-}$	τ_m-SSC 3m	4m	5m	6m	7m	8m	9m	10m	11m
τ_m-SSC 3m		ns	ns	ns	ns	**	***	****	***
4m			ns	ns	ns	ns	ns	*	ns
5m				ns	ns	ns	**	**	*
6m					ns	ns	*	*	*
7m						ns	ns	ns	ns
8m							ns	ns	ns
9m								ns	ns
10m									ns
11m									

τ_m LSC

B6 (WT)	τ_m-LSC 3m	4m	5m	6m	7m	8m	9m	10m	11m
τ_m-LSC 3m		ns	ns	*	**	**	***	****	****
4m			ns	ns	ns	*	**	****	****
5m				ns	ns	ns	ns	*	**
6m					ns	ns	ns	ns	*
7m						ns	ns	ns	ns
8m							ns	ns	ns
9m								ns	ns
10m									ns
11m									

ApoE$^{-/-}$	τ_m-LSC 3m	4m	5m	6m	7m	8m	9m	10m	11m
τ_m-LSC 3m		ns	ns	ns	**	****	***	****	***
4m			ns	ns	*	***	**	****	**
5m				ns	ns	**	ns	**	*
6m					ns	ns	**	****	****
7m						ns	ns	ns	ns
8m							ns	ns	ns
9m								ns	ns
10m									ns
11m									

Nrf2$^{-/-}$	τ_m-LSC 3m	4m	5m	6m	7m	8m	9m	10m	11m
τ_m-LSC 3m		ns	ns	ns	ns	*	*	***	ns
4m			ns	ns	ns	ns	ns	ns	ns
5m				ns	ns	ns	ns	**	ns
6m					ns	ns	ns	ns	ns
7m						ns	ns	ns	ns
8m							ns	ns	ns
9m								ns	ns
10m									ns
11m									

ns, not significant.
*$P < 0.05$, **$P < 0.01$, ***$P < 0.001$, ****$P < 0.0001$.

ORO Staining

Figure 6 shows the results of ORO staining of the retina-choroid complex at 6 and 11 months. At 6 months of age, there was no significant difference in the staining, whereas at 11 months of age the ORO staining of the ApoE$^{-/-}$ mice (score mean:1.6) was significantly stronger than the WT (score mean, 0.75;

Table 3. Results of Statistical Analysis of τ_m Comparison Between Different Strains at Different Time Points

Age in Months	3 Months	4 Months	5 Months	6 Months	7 Months	8 Months	9 Months	10 Months	11 Months
SSC									
WT vs ApoE$^{-/-}$	ns	**	ns	ns	ns	ns	*	**	ns
WT vs Nrf2$^{-/-}$	ns	**	ns	ns	ns	ns	ns	ns	ns
ApoE$^{-/-}$ vs Nrf2$^{-/-}$	ns	ns	ns	ns	ns	ns	ns	ns	*
LSC									
WT vs ApoE$^{-/-}$	ns	ns	ns	ns	ns	**	ns	ns	ns
WT vs Nrf2$^{-/-}$	ns	ns	*	ns	ns	ns	ns	ns	****
ApoE$^{-/-}$ vs Nrf2$^{-/-}$	ns	ns	**	ns	*	***	*	**	****

ns, not significant.
*$P < 0.05$, **$P < 0.01$, ***$P < 0.001$, ****$P < 0.0001$.

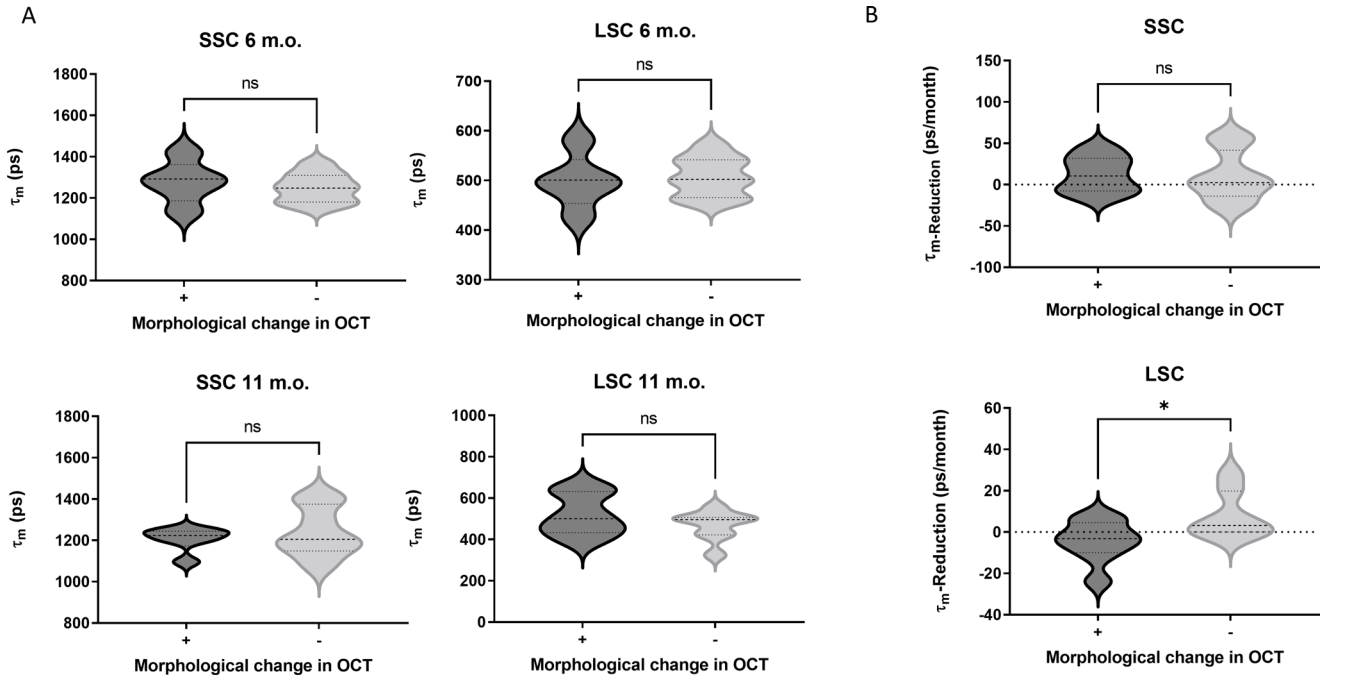

Figure 8. Comparison of τ_m at 6 and 11 m.o. between the mice with and without detected change in OCT. (**A**) Comparison of absolute τ_m value in the inner ring. (**B**) Comparison of the reduction rate of τ_m in the inner ring over time. There were no significant differences in absolute τ_m value between two groups (**A**), although there was a significant difference in the reduction rate of τ_m value at 6 months in LSC (**B**).

$P < 0.01$) and the Nrf2$^{-/-}$ mice (score mean, 0.83; $P < 0.05$).

FLIO

Goodness of Fit of FLT Decay Curves

The values of reduced χ^2 of all analyzed data were confirmed to be close to 1 for both channels; μ (mean), μ-σ, and μ + σ were 0.995 ± 0.006, 0.933 ± 0.012, and 1.061 ± 0.020 in SSC, 1.043 ± 0.009, 0.963 ± 0.009, and 1.121 ± 0.015 in LSC, respectively. A representative data of time-correlated single photon counting data together with the fitted curve is shown Supplementary Fig. S1. Furthermore, as shown as an example in the supplemental data, the difference in reduced χ^2 values between two-component and three-component fitting was negligibly small. Therefore, two-component fitting was used in this study.

FLT in SSC

In a previous study, it was shown that the mean FLT (τ_m) of the mouse fundus decreases with age.[20] This finding is consistent with our general observation in the current study. As shown in Figure 7A, the τ_m of WT decreased steadily during the study period (from 1370 ps ± 65 at 3 months to 1195 ps ± 47 at 11 months; $P <$ 0.0001). Similarly, the FLT of the model mice shortened significantly as well (ApoE$^{-/-}$ mice, from 1372 ± 71 ps to 1140 ± 71 ps [$P < 0.0001$]; Nrf2$^{-/-}$ mice, from 1334 ± 100 ps to 1207 ± 85 ps [$P < 0.001$]). At 4 months of age, the τ_m of the model mice was significantly shorter than that of WT; otherwise, there was no difference among the three strains up to 8 months. There was no significant difference in the τ_m between WT and Nrf2$^{-/-}$ mice until 11 months. In contrast, the τ_m of the ApoE$^{-/-}$ mice shortened more substantially over time and showed a significant difference from τ_m of WT in the later months (Fig. 7A and C and Tables 1–3).

FLT in LSC

As shown in Figure 7B, like in the SSC, the τ_m of the WT mice decreased significantly during the study period in LSC as well (from 539 ± 66 ps to 407 ± 54 ps; $P < 0.0001$). In the two AMD mouse models, the τ_m in LSC progressed inversely over time; ApoE$^{-/-}$ mice started shortening substantially from 7 months of age, whereas τ_m of the Nrf2$^{-/-}$ mice did not shorten like the other two strains. This factor led to significant differences in τ_m between ApoE$^{-/-}$ mice and WT mice at 8 months, between ApoE$^{-/-}$ mice and Nrf2$^{-/-}$ mice at all times after 8 months (Fig. 7B and D and Tables 1–3).

Relation Between OCT Changes and τ_m

To evaluate the relationship between the presence or absence of OCT changes and τ_m, the τ_m at 6 and 11 months of age was compared for the group with and without changes in OCT. The results showed that there was no significant difference between the absolute value of τ_m and the presence of OCT changes (Fig. 8A). However, the rate of decrease in τ_m over time was significantly less in LSC in the group with OCT change than in the group without OCT change (Fig. 8B).

Discussion

AMD is multifactorial[23] and polygenic, and animal models have been created at the laboratory level to present different human AMD characteristics, although they are not etiologically representative of human AMD. According to the known molecular pathogenesis of AMD, there are different approaches to create models; with complement pathway, such as complement factor H knock out ($Cfh^{-/-}$) mice,[24] inflammatory chemokines, such as chemokine ligand 2 knock out ($Ccl2^{-/-}$) mice,[25] lipid and glucose metabolism, such as $ApoE^{-/-}$ mice,[26] or oxidative stress, such as $Nrf2^{-/-}$ mice.[16]

Regarding impaired lipid metabolism, AMD in humans has been shown to be associated with mutations in several cholesterol-related genes, including ApoE, hepatic lipase, cholesteryl ester transfer protein, lipoprotein lipase, and ATP-binding cassette transporter A1.[27,28] ApoE is primarily expressed in retinal ganglion cells, Müller cells, and the RPE.[29,30] It is a glycoprotein and part of lipoprotein particles, which are essentially involved in regulation of cholesterol metabolism and lipid transport in neural tissues.[31] Furthermore, it is suggested to play an important role in subretinal inflammation possibly through interleukin-6.[26] Human APOE exists in three isoforms, form E2, E3 and E4. Dysfunction of ApoE, especially ApoE e4 allele, has been shown to play an important role in the pathogenesis of Alzheimer's disease.[32] Contrarily, ApoE e4 allele might have a protective effect in AMD development.[33] ApoE2 has been noted to potentially increase the risk of AMD, which is still controversially discussed.[34,35] Moreover, ApoE is one of the major components of drusen.[31] For these reasons, manipulation of the ApoE gene was proposed as a fruitful approach to producing drusen with high esterified cholesterol in laboratory animals.[36] $ApoE^{-/-}$ mice did, in fact, exhibit similar ultrastructure to basal linear deposit in Bruch's membrane.[15]

However, the influence of ApoE deficiency in mouse retinal function has been shown to be quite mild, and it can be exacerbated only under high cholesterol diet.[15,37,38] As the reason of this fact, mice have only one ApoE isoform and one possible compensatory mechanism might induce increased expression of ApoA4, a potent inhibitor of lipid oxidation, which may protect the retina from cholesterol oxidation.[39,40]

Nrf $2^{-/-}$mice, in contrast, have shown AMD-like findings such as Drusen-like deposits, accumulation of lipofuscin or CNV more frequently. The nuclear factor Nrf2 is located at the transcriptional level of RPE cells. There, erythroid-2 related factor 2 regulates the activity of antioxidant enzymes such as catalase and superoxide dismutase as well as the cellular concentration levels of glutathione and thioredoxins.[41] If the expression of Nrf2 is switched off, as in the $Nrf2^{-/-}$ mice, oxidative stress in the RPE tissue increases to pathological levels and can reach cell-damaging levels[42], which can then lead to AMD development. Richert et al.[43] reported a significant influence of the mutation of crumbs homolog 1 (CRB1) gene in macular degeneration phenotype of $Nrf2^{-/-}$ mice. We cannot rule out the possibility that the $Nrf2^{-/-}$ mice we used also had a different genetic background with respect to the crb1 gene. Unfortunately, we had no information on this when we purchased the animals, and we did not examine them ourselves; thus, this information remains unknown.

In light of the description of pathology and phenotype in both transgenic mice described elsewhere in this article, the results of OCT, lipid staining, and blood TAC measurements in this study would be reasonable and explainable. In OCT, the number of $ApoE^{-/-}$ mice showing abnormalities was clearly lower than that of $Nrf2^{-/-}$ mice. The ORO lipid staining at the Bruch's membrane was strongest in the $ApoE^{-/-}$ mice and increased with age. Zhao et al[44] could detect thickened Bruch's membrane also in Nrf $2^{-/-}$mice, but it starts from the age of 12 months. TAC level was increased significantly in $ApoE^{-/-}$ mice, which is strongly assumed to be due to the compensatory mechanisms including ApoA4 described elsewhere in this article and also probably upregulation of other antioxidants. $Nrf2^{-/-}$ mice showed a tendentially higher TAC than the WT, but there was no significant difference. Because Nrf2 is a key transcriptional regulator of antioxidant, its compensatory mechanisms are expected to be less likely to function strongly.

Those differences might be related essentially to the difference in τ_m between both models. Compared with the τ_m of the human fundus, the τ_m of mouse fundus were generally longer in both spectral channels, especially in SSC. Furthermore, the τ_m decreased over

time in all three mouse strains, which is consistent with the previous results.[20] The reason for this is not yet clearly understood, but melanin accumulation could be among the possible causes. Melanin has reportedly a relative short τ_m of 100 to 200 ps.[45–47] In the SSC, the τ_m was the shortest in ApoE$^{-/-}$ mice at each point in time. In LSC, ApoE$^{-/-}$ mice still showed the shortest τ_m at most times compared with WT, whereas the τ_m of Nrf 2$^{-/-}$ mice was longer than the one of WT at almost every time of measurement. This result led to partly clear significant differences between both AMD mouse models.

It has been shown that drusen itself does not have a significant effect on τ_m,[48] and increased intracellular lipofuscin is associated with prolonged τ_m, especially in the LSC.[49] Given these points, it is likely that the τ_m is not related significantly to lipid deposition under the RPE in ApoE$^{-/-}$ mice, but rather to an increase in cellular metabolism related to the compensatory mechanisms, as also implied by the increased TAC. Data from basic studies suggest that τ_m is prolonged under conditions of reduced mitochondrial function and, conversely, shortened under conditions of increased activation under mild stress (Kubota et al. *IOVS* 2022;63:ARVO E-Abstract 2471). It is conceivable that ApoE$^{-/-}$ mice up to 11 months of age might have been able to maintain high cellular activity primarily owing to the compensatory mechanism. Other causes, such as the condition of the lens, did not differ between groups, as far as we could observe.

A possible mechanism for τ_m shortening during hypermetabolism has been suggested to be related to changes in the τ_m of flavin adenin dinucleotide and flavin mononucleotide, cofactors in different intracellular metabolic reactions.[50,11] The change in the protein binding states of theses cofactors may vary under different cellular metabolic states, which may lead to the change in the τ_m. This theory requires further discussion, but in any case, we cannot rule out the possibility that the τ_m is shortened in the very early stages of degenerative retinal disorders, when cellular function is still in a compensatory state.

It is likely that the relative τ_m prolongation observed in LSC in Nrf2$^{-/-}$ mice is due to increased intracellular lipofuscin. The τ_m of lipofuscin has been reported to be longer than 1000 ps,[8,51] and it is suggested that this factor is related to an age-related increase in the τ_m of LSC in humans.[10,13] Suppression of cellular antioxidant function results in direct oxidative stress on cells, which leads to suppression of intracellular energy metabolism and organelle function, resulting in an increase in lipofuscin. This process is known to be an early factor of pathogenesis of aging and AMD.[52] Abnormalities in lipid metabolism in ApoE$^{-/-}$ mice should not directly lead to lipofuscin accumulation unless it results in impaired cellular function.

Limitations of this study are the lack of possibility to directly translate the results to the human fundus. On the one hand, as described elsewhere in this article, no model can fully represent diseases of the human eye and τ_m in mouse fundus differs from that of human fundus.[53] In contrast, FLIO was not constructed for the measurement of mice and this might lead to a discrepancy in spatial resolution of FLIO images owing to optic aberration of the mouse eye.

Furthermore, even though the results show statistic significances and we already explained that there may be biological causes for this finding, it must be kept in mind that also the variability of the measures themselves may have contributed to the results of this particular series of experiments.

Another point of limitation is the termination of the study at month 11. This factor might restrict the findings to early states of AMD. Observation over a longer period of time could detect long-term changes.

In conclusion, our study showed that two mouse models of AMD with different metabolic states exhibit significantly different FLTs. Although there are some limitations and the detailed mechanism requires further study, it is suggested that FLIO may indicate different retinal metabolic states in early AMD.

Acknowledgments

The authors thank Jonas Obleser in Physiological Psychology and Research Methods at the University of Lübeck for his advice on biometric planning for animal study, and we thank Christine Örün in the Department of Ophthalmology at the University of Lübeck for her technical support in histological assessments.

Funded by Federal Ministry of Education and Research (BMBF: Grant #:13N14444, 13N14445).

Disclosure: **S.R. Sonntag,** None; **B. Klein,** None; **R. Brinkmann,** None; **S. Grisanti,** None; **Y. Miura,** None

References

1. Congdon N, O'Colmain B, Klaver CCW, et al. Causes and prevalence of visual impairment among adults in the United States. *Arch Ophthalmol Chic*. 2004;122(4):477–485.

2. Schutt F, Davies S, Kopitz J, Holz FG, Boulton ME. Photodamage to human RPE cells by A2-E, a retinoid component of lipofuscin. *Invest Ophthalmol Vis Sci*. 2000;41(8):2303–2308.
3. Datta S, Cano M, Ebrahimi K, Wang L, Handa JT. The impact of oxidative stress and inflammation on RPE degeneration in non-neovascular AMD. *Prog Retin Eye Res*. 2017;60:201–218.
4. Potilinski MC, Tate PS, Lorenc VE, Gallo JE. New insights into oxidative stress and immune mechanisms involved in age-related macular degeneration tackled by novel therapies. *Neuropharmacology*. 2021;188:108513.
5. Tsai YT, Li Y, Ryu J, et al. Impaired cholesterol efflux in retinal pigment epithelium of individuals with juvenile macular degeneration. *Am J Hum Genet*. 2021;108(5):903–918.
6. Gouras P, Ivert L, Neuringer M, Nagasaki T. Mitochondrial elongation in the macular RPE of aging monkeys, evidence of metabolic stress. *Graefes Arch Clin Exp Ophthalmol*. 2016;254(6):1221–1227.
7. Zhan J, He J, Zhou Y, et al. Crosstalk between the autophagy-lysosome pathway and the ubiquitin-proteasome pathway in retinal pigment epithelial cells. *Curr Mol Med*. 2016;16(5):487–495.
8. Schweitzer D, Schenke S, Hammer M, et al. Towards metabolic mapping of the human retina. *Microsc Res Techniq*. 2007;70(5):410–419.
9. Dysli C, Wolf S, Berezin MY, Sauer L, Hammer M, Zinkernagel MS. Fluorescence lifetime imaging ophthalmoscopy. *Prog Retin Eye Res*. 2017;60:120–143.
10. Sauer L, Vitale AS, Modersitzki NK, Bernstein PS. Fluorescence lifetime imaging ophthalmoscopy: autofluorescence imaging and beyond. *Eye (Lond)*. 2021;35(1):93–109.
11. Kalinina S, Freymueller C, Naskar N, et al. Bioenergetic alterations of metabolic redox coenzymes as NADH, FAD and FMN by means of fluorescence lifetime imaging techniques. *Int J Mol Sci*. 2021;22(11):5952.
12. Schweitzer D, Deutsch L, Klemm M, et al. Fluorescence lifetime imaging ophthalmoscopy in type 2 diabetic patients who have no signs of diabetic retinopathy. *J Biomed Opt*. 2015;20(6):61106.
13. Sauer L, Gensure RH, Andersen KM, et al. Patterns of fundus autofluorescence lifetimes in eyes of individuals with nonexudative age-related macular degeneration. *Invest Ophthalmol Vis Sci*. 2018;59(4):Amd65–Amd77.
14. Sonntag SR, Kreikenbohm M, Bohmerle G, Stagge J, Grisanti S, Miura Y. Impact of cigarette smoking on fluorescence lifetime of ocular fundus. *Sci Rep*. 2023;13(1):11484.
15. Dithmar S, Curcio CA, Le NA, Brown S, Grossniklaus HE. Ultrastructural changes in Bruch's membrane of apolipoprotein E-deficient mice. *Invest Ophthalmol Vis Sci*. 2000;41(8):2035–2042.
16. Zhao Z, Chen Y, Wang J, et al. Age-related retinopathy in NRF2-deficient mice. *PLoS One*. 2011;6(4):e19456.
17. Piedrahita JA, Zhang SH, Hagaman JR, Oliver PM, Maeda N. Generation of mice carrying a mutant apolipoprotein E gene inactivated by gene targeting in embryonic stem cells. *Proc Natl Acad Sci USA*. 1992;89(10):4471–4475.
18. Chan K, Lu R, Chang JC, Kan YW. NRF2, a member of the NFE2 family of transcription factors, is not essential for murine erythropoiesis, growth, and development. *Proc Natl Acad Sci USA*. 1996;93(24):13943–13948.
19. Becker W. Fluorescence lifetime imaging–techniques and applications. *J Microsc*. 2012;247(2):119–136.
20. Dysli C, Dysli M, Enzmann V, Wolf S, Zinkernagel MS. Fluorescence lifetime imaging of the ocular fundus in mice. *Invest Ophthalmol Vis Sci*. 2014;55(11):7206–7215.
21. Teister J, Liu A, Wolters D, Pfeiffer N, Grus FH. Peripapillary fluorescence lifetime reveals age-dependent changes using fluorescence lifetime imaging ophthalmoscopy in rats. *Exp Eye Res*. 2018;176:110–120.
22. Wang Y, Goulart RA, Pantanowitz L. Oil red O staining in cytopathology. *Diagn Cytopathol*. 2011;39(4):272–273.
23. Fleckenstein M, Keenan TDL, Guymer RH, et al. Age-related macular degeneration. *Nat Rev Dis Primers*. 2021;7(1):31.
24. Ding JD, Kelly U, Landowski M, et al. Expression of human complement factor H prevents age-related macular degeneration-like retina damage and kidney abnormalities in aged Cfh knockout mice. *Am J Pathol*. 2015;185(1):29–42.
25. Chan CC, Ross RJ, Shen D, et al. Ccl2/Cx3cr1-deficient mice: an animal model for age-related macular degeneration. *Ophthalmic Res*. 2008;40(3-4):124–128.
26. Levy O, Lavalette S, Hu SJ, et al. APOE isoforms control pathogenic subretinal inflammation in age-related macular degeneration. *J Neurosci*. 2015;35(40):13568–13576.
27. Fritsche LG, Fariss RN, Stambolian D, Abecasis GR, Curcio CA, Swaroop A. Age-related macular degeneration: genetics and biology coming

together. *Annu Rev Genom Hum G*. 2014;15:151–171.
28. Shughoury A, Sevgi DD, Ciulla TA. Molecular genetic mechanisms in age-related macular degeneration. *Genes (Basel)*. 2022;13(7):1233.
29. Amaratunga A, Abraham CR, Edwards RB, Sandell JH, Schreiber BM, Fine RE. Apolipoprotein E is synthesized in the retina by Muller glial cells, secreted into the vitreous, and rapidly transported into the optic nerve by retinal ganglion cells. *J Biol Chem*. 1996;271(10):5628–5632.
30. Anderson DH, Ozaki S, Nealon M, et al. Local cellular sources of apolipoprotein E in the human retina and retinal pigmented epithelium: implications for the process of drusen formation. *Am J Ophthalmol*. 2001;131(6):767–781.
31. Mahley RW. Apolipoprotein E: cholesterol transport protein with expanding role in cell biology. *Science*. 1988;240(4852):622–630.
32. Serrano-Pozo A, Das S, Hyman BT. APOE and Alzheimer's disease: advances in genetics, pathophysiology, and therapeutic approaches. *Lancet Neurol*. 2021;20(1):68–80.
33. Malek G, Johnson LV, Mace BE, et al. Apolipoprotein E allele-dependent pathogenesis: a model for age-related retinal degeneration. *Proc Natl Acad Sci USA*. 2005;102(33):11900–11905.
34. Souied EH, Benlian P, Amouyel P, et al. The epsilon 4 allele of the apolipoprotein E gene as a potential protective factor for exudative age-related macular degeneration. *Am J Ophthalmol*. 1998;125(3):353–359.
35. McKay GJ, Patterson CC, Chakravarthy U, et al. Evidence of association of APOE with age-related macular degeneration: a pooled analysis of 15 studies. *Hum Mutat*. 2011;32(12):1407–1416.
36. Wang L, Clark ME, Crossman DK, et al. Abundant lipid and protein components of drusen. *PLoS One*. 2010;5(4):e10329.
37. Ong JM, Zorapapel NC, Rich KA, et al. Effects of cholesterol and apolipoprotein E on retinal abnormalities in ApoE-deficient mice. *Invest Ophthalmol Vis Sci*. 2001;42(8):1891–1900.
38. Ong JM, Zorapapel NC, Aoki AM, et al. Impaired electroretinogram (ERG) response in apolipoprotein E-deficient mice. *Curr Eye Res*. 2003;27(1):15–24.
39. Ostos MA, Conconi M, Vergnes L, et al. Antioxidative and antiatherosclerotic effects of human apolipoprotein A-IV in apolipoprotein E-deficient mice. *Arterioscl Throm Vas*. 2001;21(6):1023–1028.
40. Saadane A, Petrov A, Mast N, et al. Mechanisms that minimize retinal impact of apolipoprotein E absence. *J Lipid Res*. 2018;59(12):2368–2382.
41. Tonelli C, Chio IIC, Tuveson DA. Transcriptional regulation by Nrf2. *Antioxid Redox Signal*. 2018;29(17):1727–1745.
42. Sachdeva MM, Cano M, Handa JT. Nrf2 signaling is impaired in the aging RPE given an oxidative insult. *Exp Eye Res*. 2014;119:111–114.
43. Richert E, Klettner A, von der Burchard C, Roider J, Tode J. CRB1(rd8) mutation influences the age-related macular degeneration phenotype of NRF2 knockout mice and favors choroidal neovascularization. *Adv Med Sci*. 2020;65(1):71–77.
44. Zhao J, Liao Y, Chen J, et al. Aberrant buildup of all-trans-retinal dimer, a nonpyridinium bisretinoid lipofuscin fluorophore, contributes to the degeneration of the retinal pigment epithelium. *Invest Ophthalmol Vis Sci*. 2017;58(2):1063–1075.
45. Dimitrow E, Riemann I, Ehlers A, et al. Spectral fluorescence lifetime detection and selective melanin imaging by multiphoton laser tomography for melanoma diagnosis. *Exp Dermatol*. 2009;18(6):509–515.
46. Miura Y, Huettmann G, Orzekowsky-Schroeder R, et al. Two-photon microscopy and fluorescence lifetime imaging of retinal pigment epithelial cells under oxidative stress. *Invest Ophthalmol Vis Sci*. 2013;54(5):3366–3377.
47. Hammer M, Sauer L, Klemm M, Peters S, Schultz R, Haueisen J. Fundus autofluorescence beyond lipofuscin: lesson learned from ex vivo fluorescence lifetime imaging in porcine eyes. *Biomed Opt Express*. 2018;9(7):3078–3091.
48. Schwanengel LS, Weber S, Simon R, et al. Changes in drusen-associated autofluorescence over time observed by fluorescence lifetime imaging ophthalmoscopy in age-related macular degeneration. *Acta Ophthalmol*. 2023;101(2):e154–e166.
49. Sauer L, Vitale AS, Milliken CM, Modersitzki NK, Blount JD, Bernstein PS. Autofluorescence lifetimes measured with fluorescence lifetime imaging ophthalmoscopy (FLIO) are affected by age, but not by pigmentation or gender. *Transl Vis Sci Technol*. 2020;9(9):2.
50. Nakashima N, Yoshihara K, Tanaka F, Yagi K. Picosecond fluorescence lifetime of the coenzyme of D-amino acid oxidase. *J Biol Chem*. 1980;255(11):5261–5263.
51. Yakovleva MA, Feldman TB, Arbukhanova PM, Borzenok SA, Kuzmin VA, Ostrovsky MA. The fluorescence lifetime of lipofuscin granule fluo-

rophores contained in the retinal pigment epithelium cells from human cadaver eyes in normal state and in the case of visualized pathology. *Dokl Biochem Biophys*. 2017;474(1):239–243.

52. Deng Y, Qiao L, Du M, et al. Age-related macular degeneration: epidemiology, genetics, pathophysiology, diagnosis, and targeted therapy. *Genes Dis*. 2022;9(1):62–79.
53. Dysli C, Dysli M, Wolf S, Zinkernagel M. Fluorescence lifetime distribution in phakic and pseudophakic healthy eyes. *PLoS One*. 2023;18(1):e0279158.